AGU PUBLICATIONS

JGR

Journal of Geophysical Research: Space Physics

RESEARCH ARTICLE

10.1002/2017JA024169

Key Points:

- New evidence for EMIC-driven rapid loss of radiation belt relativistic electrons is provided by an event study
- Quasi-monotonic radial profile of relativistic electron phase space density formed because of the combination of radial and local loss processes
- Relativistic electron flux showed a dip structure closely related to intense EMIC waves

Correspondence to:
Z. Su,
szpe@mail.ustc.edu.cn

Citation:
Su, Z., Gao, Z., Zheng, H., Wang, Y., Wang, S., Spence, H. E., … Wygant, J. R. (2017). Rapid loss of radiation belt relativistic electrons by EMIC waves. *Journal Geophysical Research: Space Physics*, *122*. https://doi.org/10.1002/2017JA024169

Received 20 MAR 2017
Accepted 27 AUG 2017
Accepted article online 31 AUG 2017

Rapid Loss of Radiation Belt Relativistic Electrons by EMIC Waves

Zhenpeng Su[1,2], Zhonglei Gao[1,3], Huinan Zheng[1,2], Yuming Wang[1,2], Shui Wang[1,2], H. E. Spence[4], G. D. Reeves[5,6], D. N. Baker[7], and J. R. Wygant[8]

[1]CAS Key Laboratory of Geospace Environment, Department of Geophysics and Planetary Sciences, University of Science and Technology of China, Hefei, China, [2]Collaborative Innovation Center of Astronautical Science and Technology, University of Science and Technology of China, Hefei, China, [3]Mengcheng National Geophysical Observatory, School of Earth and Space Sciences, University of Science and Technology of China, Hefei, China, [4]Institute for the Study of Earth, Oceans, and Space, University of New Hampshire, Durham, NH, USA, [5]Space Science and Applications Group, Los Alamos National Laboratory, Los Alamos, NM, USA, [6]Space Sciences Division, New Mexico Consortium, Los Alamos, NM, USA, [7]Laboratory for Atmospheric and Space Physics, University of Colorado Boulder, Boulder, CO, USA, [8]School of Physics and Astronomy, University of Minnesota, Twin Cities, Minneapolis, MN, USA

Abstract How relativistic electrons are lost is an important question surrounding the complex dynamics of the Earth's outer radiation belt. Radial loss to the magnetopause and local loss to the atmosphere are two main competing paradigms. Here on the basis of the analysis of a radiation belt storm event on 27 February 2014, we present new evidence for the electromagnetic ion cyclotron (EMIC) wave-driven local precipitation loss of relativistic electrons in the heart of the outer radiation belt. During the main phase of this storm, the radial profile of relativistic electron phase space density was quasi-monotonic, qualitatively inconsistent with the prediction of radial loss theory. The local loss at low L shells was required to prevent the development of phase space density peak resulting from the radial loss process at high L shells. The rapid loss of relativistic electrons in the heart of outer radiation belt was observed as a dip structure of the electron flux temporal profile closely related to intense EMIC waves. Our simulations further confirm that the observed EMIC waves within a quite limited longitudinal region were able to reduce the off-equatorially mirroring relativistic electron fluxes by up to 2 orders of magnitude within about 1.5 h.

1. Introduction

The Earth's outer radiation belt electrons can exhibit complex dynamics during both storm (e.g., Baker et al., 1986; Friedel et al., 2002; Reeves et al., 2003; Onsager et al., 2002; Horne, Thorne, Shprits, et al., 2005; Millan & Thorne, 2007; Anderson et al., 2015) and nonstorm (Su et al., 2014, 2016; Schiller et al., 2014; Su, Zhu, Xiao, Zong, et al., 2015) times. How electrons are accelerated and lost are two fundamental questions in radiation belt science.

Radial and local acceleration processes have been proposed as two dominant paradigms for the buildup of the radiation belt relativistic electron fluxes (e.g., Schulz & Lanzerotti 1974; Horne & Thorne, 1998; Summers et al., 1998; Rostoker et al., 1998; Elkington et al., 1999; Summers et al., 2002; Meredith, Cain, et al., 2003; Horne, Thorne, Glauert, et al., 2005; Shprits, Thorne, Horne, et al., 2006; Mathie & Mann, 2000; Loto'Aniu et al., 2006; Ukhorskiy et al., 2006; Omura et al., 2015). The corresponding evidences can be classified into two categories: (1) electron phase space density (PSD) characteristics (Green & Kivelson, 2004) and (2) electron pitch angle distribution (PAD) characteristics (Horne & Thorne, 1998; Summers et al., 1998). The radial profiles of electron PSDs are monotonic under the action of radial acceleration alone (e.g., Su, Zhu, Xiao, Zong, et al., 2015) and become peaked under the action of local acceleration (e.g., Chen et al., 2007; Reeves et al., 2013). The flat-top PADs of electrons can be produced by the local acceleration (Horne et al., 2003; Thorne et al., 2013; Yang et al., 2016), but no representative PAD characteristics should be expected for radial acceleration.

Parallel to the acceleration processes, there have been two dominant loss paradigms (Albert, 2014). One paradigm (Li et al., 1997) is the radial loss to the magnetopause (boundary of the magnetosphere). With the enhancement of solar wind pressure, the magnetopause is compressed toward the Earth and electrons

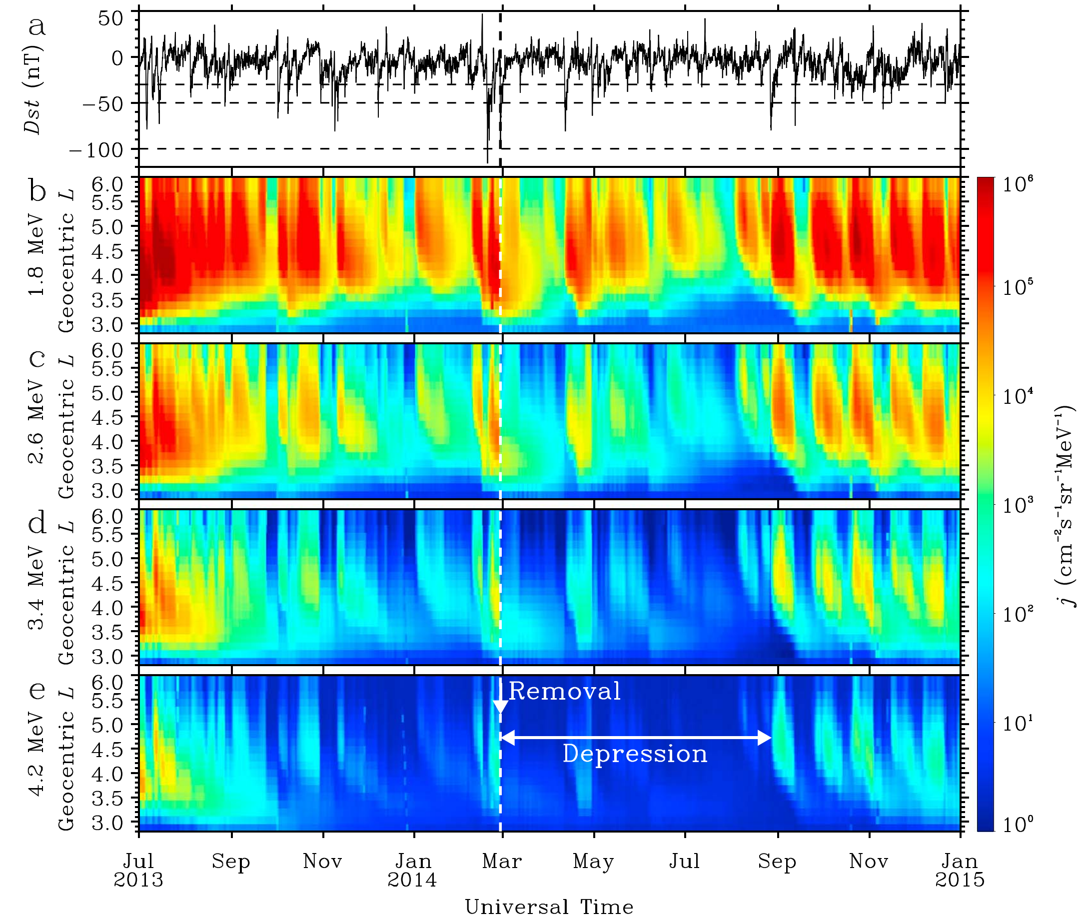

Figure 1. An 18 month overview of geospace radiation environment: (a) geomagnetic activity index *Dst* and (b–e) spin-averaged relativistic electron differential fluxes *j* (color coded) at different energy channels (shown). The vertical dashed line denotes the 27 February 2014 storm producing the rapid loss and the subsequent 6 month depression of relativistic electron radiation.

with drift paths crossing the magnetopause are directly lost (Hudson et al., 2014). Subsequently, more electrons are lost through the magnetopause due to the outward radial diffusion by ultralow frequency (ULF) waves (Shprits, Thorne, Friedel, et al., 2006; Loto'Aniu et al., 2010). The other paradigm is the local loss to the atmosphere by whistler and electromagnetic ion cyclotron (EMIC) waves (Thorne & Kennel, 1971; Horne & Thorne, 1998; Summers et al., 1998; Meredith, Thorne, et al., 2003; Bortnik et al., 2006; Li et al., 2007; Su et al., 2011a, 2012, 2013; Ni et al., 2014; Zhu et al., 2015; Gao et al., 2016; Mourenas et al., 2016; Wang et al., 2016). Wave-driven pitch angle scattering can reduce the altitudes of electron mirror points, and collisions with atmospheric particles yield the precipitation loss of electrons. The primary characteristic of radial loss is a radially peaked PSD profile (Turner et al., 2012; Mann et al., 2016), while the main evidences for local loss are the flat-top PAD characteristic (Usanova et al., 2014; Engebretson et al., 2015; Su et al., 2016; Shprits et al., 2016) and the wave-related electron precipitation observed at low altitudes (Lorentzen et al., 2001; Millan et al., 2002; Miyoshi et al., 2008; Tsurutani et al., 2013; Breneman et al., 2015; Zhang, Halford, et al., 2016).

In this study, on the basis of the analysis of an extreme radiation belt electron loss event observed by the Van Allen Probes (Radiation Belt Storm Probes, RBSP) (Mauk et al., 2013) and the Polar-Orbiting Environmental Satellites (POES) (Evans & Greer, 2000) on 27 February 2014, we present new evidence for the EMIC-driven local precipitation loss of relativistic electrons in the heart of the outer radiation belt.

2. Event Overview

Figure 1 shows an overview of geospace radiation environment measured by RBSP in the time range from 1 July 2013 to 1 January 2015. The relativistic electron fluxes were observed by the Relativistic Electron-Proton

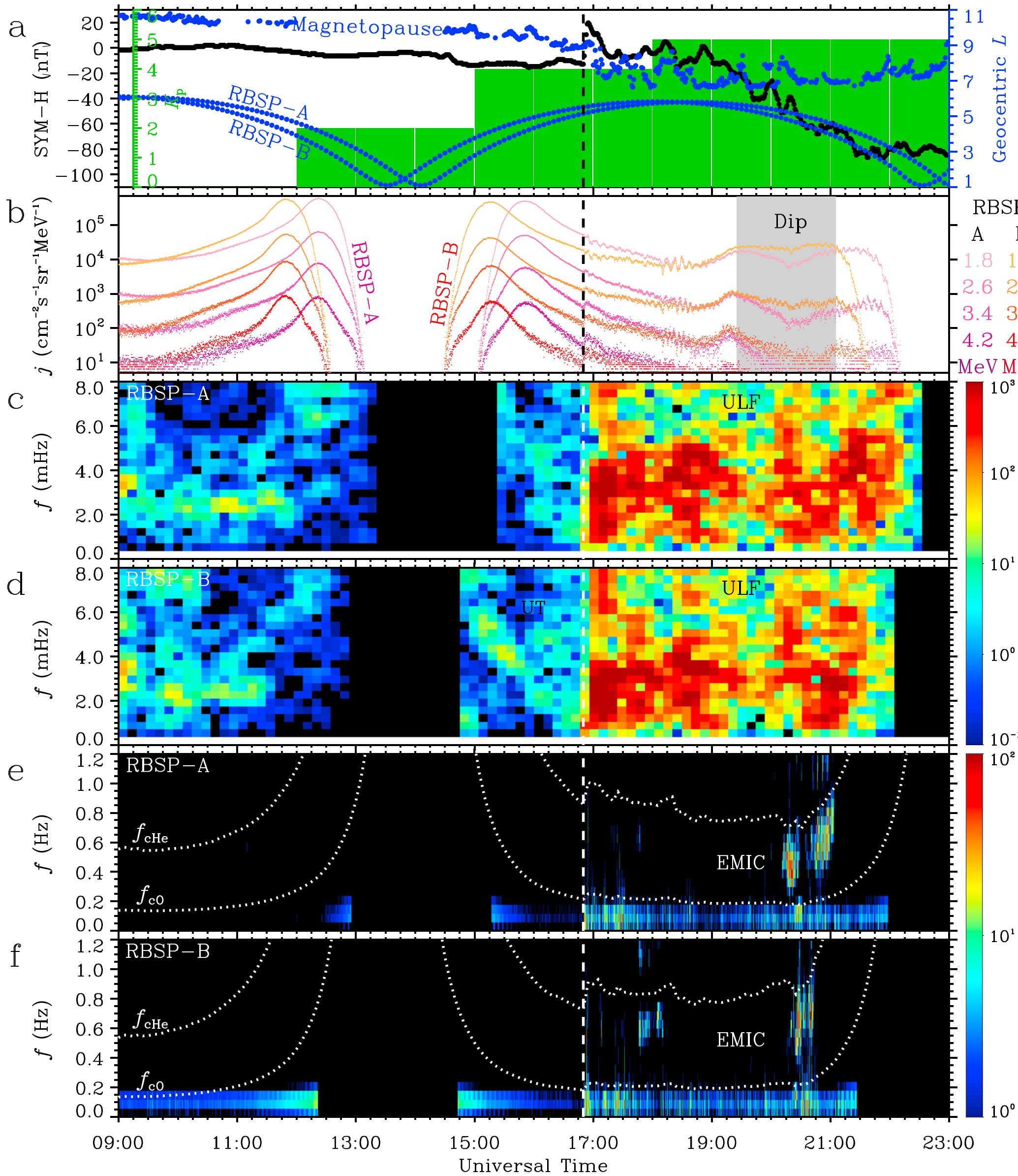

Figure 2. An overview of the 27 February 2014 radiation belt storm event: (a) geomagnetic activity indices *SYM-H* and K_p and radial locations L of subsolar magnetopause (Shue et al., 1998) and twin RBSP; (b) spin-averaged relativistic electron differential fluxes j (color coded according to energy); (c, d) power spectral density P_E of the y component ULF wave electric fields in the mGSE coordinate system (Wygant et al., 2013) as a function of time and frequency; and (e, f) power spectral density P_B of the EMIC wave magnetic fields as a function of time and frequency. In Figure 2b, the gray shadow marks the electron flux dip closely associated with intense EMIC waves. In Figures 2e and 2f, the dotted lines represent the equatorial gyrofrequencies of helium f_{cHe} and oxygen f_{cO} ions. The corresponding equatorial magnetic field B_e is estimated as $B_e = B_o B_{Me}/B_{Mo}$ with the observed local magnetic field B_o and the TS04-modeled (Tsyganenko & Sitnov, 2005) ratio B_{Me}/B_{Mo} between equatorial and local magnetic field strengths.

Telescope (REPT) (Baker et al., 2013) of Energetic Particle, Composition, and Thermal Plasma (ECT) suite (Spence et al., 2013). In response to geomagnetic storms (Figure 1a), the radiation belt relativistic electron fluxes exhibited significant variations (Figures 1b–1e). One of the most striking storms occurred on 27 February 2014 with a moderate geomagnetic disturbance level (*Dst* minimum of −85 nT). After this storm, the electron fluxes in the energy range 1.8–4.2 MeV decreased by up to 2 orders of magnitude. Even though at lower energies, the belts were reformed (Reeves et al., 2016), at 4.2 MeV the belts disappeared completely. In the following 6 months even with a spate of storms, relativistic electron fluxes were always below the level in mid-February 2014. This event on 27 February 2014 provided a good opportunity to understand

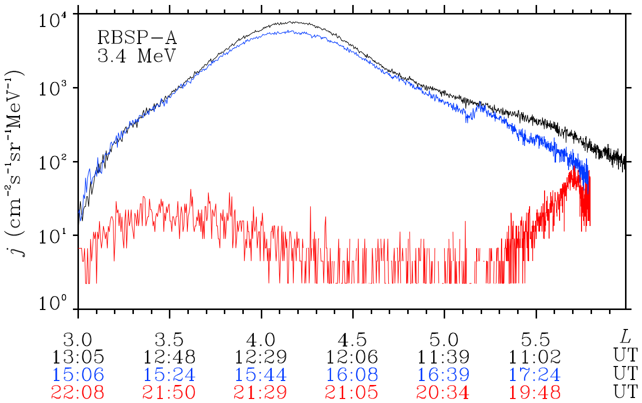

Figure 3. Radial profiles of spin-averaged relativistic electron differential fluxes j at the energy channel of 3.4 MeV (color coded according to time).

the physical mechanisms responsible for the rapid loss of relativistic electrons. Zhang, Li, et al. (2016) have analyzed the relativistic electron dynamics in the initial phase of this storm, and we here focus on the rapid loss of relativistic electrons in the main phase of this storm.

The storm started with a sudden enhancement of geomagnetic activity indices and a strong compression of magnetopause at 16:50 UT and reached its peak disturbance level around 23:00 UT (Figure 2a). In order to obtain the ULF and EMIC wave power, we perform the fast Fourier transform of both the electric field detected by the Electric Field and Wave instrument (Wygant et al., 2013) and the magnetic field detected by the tri-axial fluxgate magnetometer of the Electric and Magnetic Field Instrument and Integrated Science (EMFISIS) suite (Kletzing et al., 2013). The electron fluxes (Figure 2b) behaved quite smoothly during the quiescent period and became oscillating (Su, Zhu, Xiao, Zong, et al., 2015) due to ULF waves (Figures 2c and 2d) during the storm time. The most clear loss feature was the "dip" structure of electron fluxes observed by the twin RBSP in the heart of the outer radiation belt ($L \approx 4.5$). In contrast to the enhanced ULF waves occurring throughout the storm period, the EMIC waves mainly in the helium band showed a strong correspondence to the dip structure, implying the important role of EMIC wave-driven precipitation loss in the heart of the outer radiation belt. It should be emphasized that the electron flux profiles in Figure 2b were measured by the moving satellites. Following the interplanetary shock, the seeming decrease of electron fluxes was predominantly associated with the outward movement of satellites rather than some real loss processes. Figure 3 displays the radial profiles of 3.4 MeV electron fluxes at different time periods. One can easily find that the relativistic electrons were lost primarily in the dip period (red line, 19:25–21:05 UT) rather than following the interplanetary shock (blue line, after 16:50 UT).

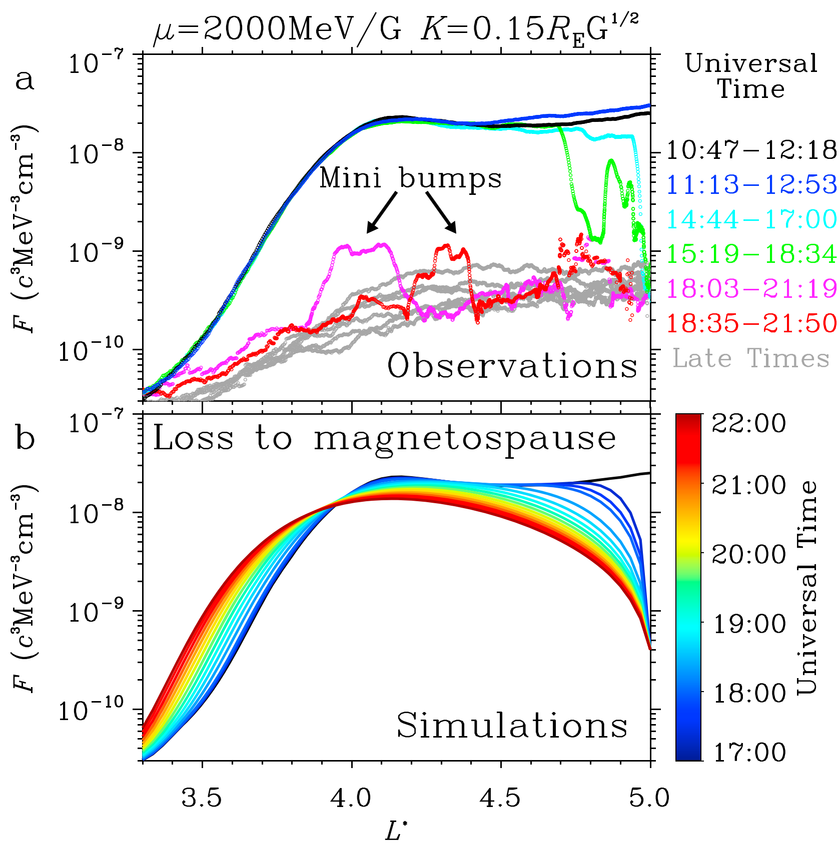

Figure 4. Comparison of observation with simulation of loss to magnetopause: (a) observation of L^*-dependent phase space density F in the TS04 geomagnetic field model (Tsyganenko & Sitnov, 2005) and (b) simulations of L^*-dependent phase space density F with diffusion rate $\langle D_{L^*L^*} \rangle = \langle D^{BA}_{L^*L^*} \rangle$. Circles and lines are color coded according to time.

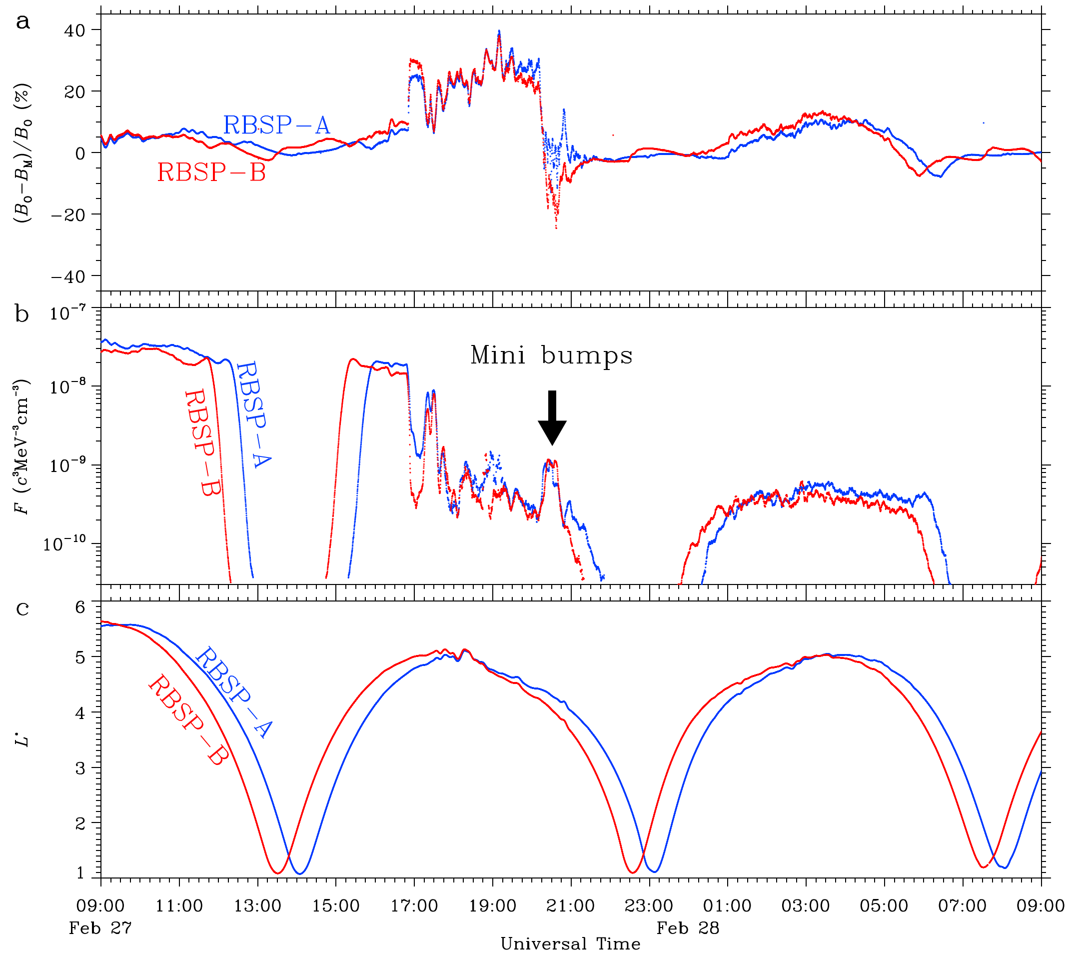

Figure 5. Generation of minibumps of electron phase space density: (a) relative difference between RBSP-observed B_O and TS04-modeled B_M geomagnetic fields, (b) electron phase space density F at $\mu = 2000$ MeV G^{-1} and $K = 0.15\ R_E$ G$^{1/2}$, and (c) magnetic shell L^*. Color helps differentiate between RBSP-A and RBSP-B satellites.

3. Radial Loss to the Magnetopause

In order to distinguish between radial loss to the magnetopause and local loss to the atmosphere, we compare the relativistic electron PSDs (Figure 4) observed with simulated in the adiabatic invariant coordinate system (μ, K, L^*). The TS04 geomagnetic field model (Tsyganenko & Sitnov, 2005) is used to calculate K and L^*, and the observed magnetic field strength is adopted to calculate μ. The plotted L^*-dependent profiles had the fixed $\mu = 2000$ MeV G^{-1} and $K = 0.15\ R_E$G$^{1/2}$. The corresponding electron energies were about 2.0 MeV at L^*=5.0 and 5.0 MeV at $L^* = 3.0$, and the corresponding local pitch angles were 40°–80°.

The observed PSDs (Figure 4a) peaked around $L^* = 4.1$ before the storm (black and blue). At the beginning of the storm (cyan and blue), a prompt and pronounced decrease of PSDs occurred at $L^* > 4.8$ resulting from the direct loss to the magnetopause (Figure 2a). The electron PSD turned into a quasi-monotonically increasing function of L^* in a few hours (magenta and red) and maintained such quasi-monotonic feature during the next 10 h (gray). We argue that the minibumps at $L^* = 3.9$–4.4 (magenta and red) are not the real spatial structures but are caused by the spatial-temporal aliasing in an unrealistic geomagnetic field model. As shown in Figure 5, the electron PSDs of twin RBSP fluctuated almost synchronously with the background field particularly during the time range 17:00–22:00 UT (Figure 5). Around 20:15 UT, a rapid and significant decrease of magnetic field yielded an enhancement of electron phase space density, primarily due to the decrease of electron energy for fixed μ in the calculation. Consequently, the radial profiles of electron phase space density (Figure 4a) exhibited two minibumps at the different L^* but at the same time period. After 22:00, the observed

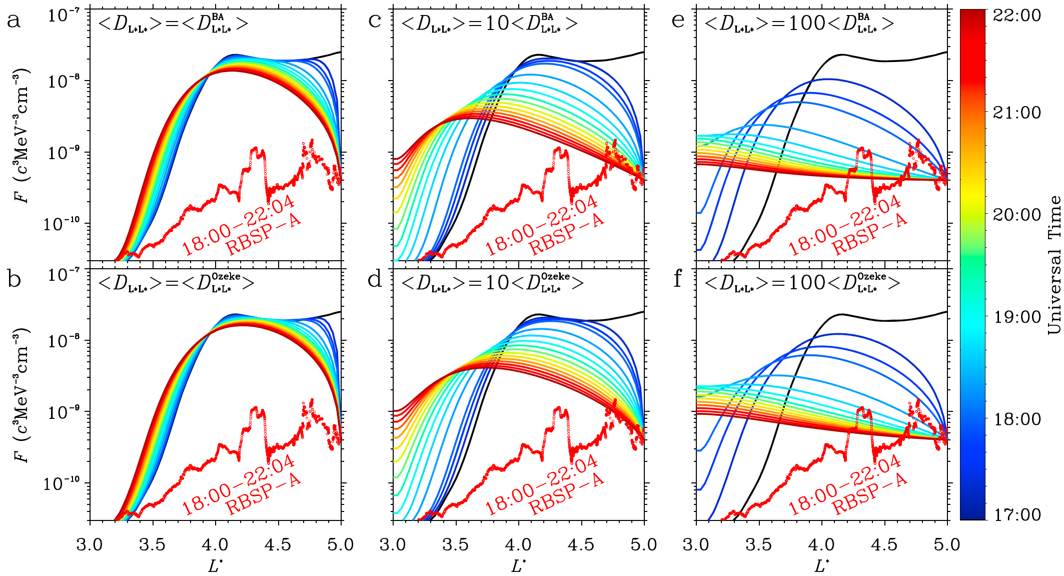

Figure 6. Comparison of observation with simulations of loss to magnetopause based on different radial diffusion rates. These panels correspond to simulations (lines color coded according to time) with radial diffusion rates (a) $\langle D_{L^*L^*}\rangle = \langle D^{BA}_{L^*L^*}\rangle$, (b) $10\langle D^{BA}_{L^*L^*}\rangle$, (c) $100\langle D^{BA}_{L^*L^*}\rangle$, (d) $\langle D^{Ozeke}_{L^*L^*}\rangle$, (e) $10\langle D^{Ozeke}_{L^*L^*}\rangle$, and (f) $100\langle D^{Ozeke}_{L^*L^*}\rangle$. Observations of RBSP-A in the time range 18:00–22:04 UT are plotted as red circles.

magnetic field was relatively smooth (Figure 5a), and the quasi-monotonic feature of the radial profiles of electron phase space density became clear (Figures 5b and 5c).

We simulate the radial diffusion of relativistic electrons (Figure 4b) by solving the equation (Schulz & Lanzerotti, 1974)

$$\frac{\partial F}{\partial t} = L^{*2}\frac{\partial}{\partial L^*}\left(\frac{\langle D_{L^*L^*}\rangle}{L^{*2}}\frac{\partial F}{\partial L^*}\right) \tag{1}$$

with the electron PSD F and the radial diffusion rate $\langle D_{L^*L^*}\rangle$. The simulation code is extracted from our previously developed STEERB model (Su et al., 2010a, 2010b, 2011b). The simulation is initialized at 17:00 UT and ended at 22:00 UT. The initial condition F_0 is given by the prestorm electron PSD of RBSP-A in the time range 11:13–12:53 UT. The boundary conditions are specified as

$$F|_{L^*=5} = 0.016F_0|_{L^*=5}, \tag{2}$$

$$\partial F/\partial L^*|_{L^*=3} = 0. \tag{3}$$

Given the RBSP orbital period of ~10 h, it is hard to differentiate between the spatial and temporal variation of ULF spectra in the time range 17:00–22:00 UT. Hence, we use the K_p-dependent radial diffusion rates developed by Brautigam and Albert (2000):

$$\langle D^{BA}_{L^*L^*}\rangle = 10^{0.506K_p-9.325}L^{*10}\ [\mathrm{d}^{-1}] \tag{4}$$

and by Ozeke et al. (2014):

$$\langle D^{Ozeke}_{L^*L^*}\rangle = 2.16\times 10^{-8}L^{*6}10^{0.217L^*+0.461K_p}\ [\mathrm{d}^{-1}]. \tag{5}$$

Prompt loss at the outer boundary $L^* = 5$ (see equation (2)) produces the negative radial gradient of PSD, allowing the outward radial diffusion at $L^* > 4.1$. In contrast, inward radial diffusion acts at $L^* < 4.1$ with the positive radial gradient. The competition between outward and inward radial diffusion results in a distinct peak of electron PSD around $L^* = 4.1$, qualitatively deviating from the observed quasi-monotonic feature. No matter how strong the radial diffusion is, the radial diffusion simulations always yield the peaked electron PSDs (Figure 6). The increase of radial diffusion strength enhances the loss of electrons at high L shells and moves the PSD peak toward low L shells. These results evidently suggest that radial diffusion alone was insufficient to explain the relativistic electron loss especially at low L shells in this event.

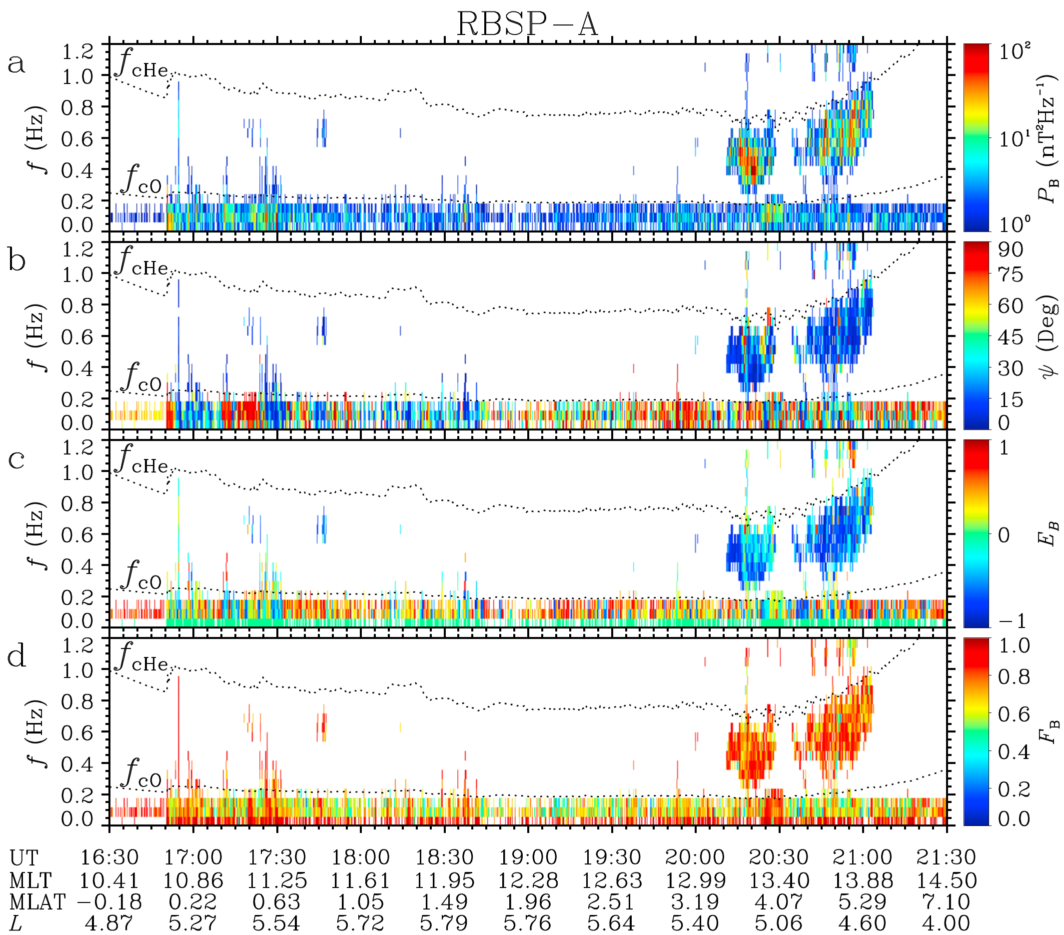

Figure 7. EMIC wave characteristics observed by RBSP-A: (a) magnetic power spectral density P_B, (b) normal angle ψ, (c) ellipticity E_B, and (d) planarity F_B. The dotted lines represent the equatorial gyrofrequencies of helium f_{cHe} and oxygen f_{cO} ions.

4. Local Loss to the Atmosphere

We next simulate the local precipitation loss of relativistic electrons in the heart of the outer radiation belt $L = 4.5$ by solving the equation (Schulz & Lanzerotti, 1974; Lyons & Williams, 1984)

$$\frac{\partial F}{\partial t} = \frac{1}{G}\frac{\partial}{\partial \alpha_e}\left[G\left(\langle D_{\alpha_e\alpha_e}\rangle\frac{\partial F}{\partial \alpha_e} + p\langle D_{\alpha_e p}\rangle\frac{\partial F}{\partial p}\right)\right] + \frac{1}{G}\frac{\partial}{\partial p}\left[Gp\left(\langle D_{p\alpha_e}\rangle\frac{\partial F}{\partial \alpha_e} + p\langle D_{pp}\rangle\frac{\partial F}{\partial p}\right)\right] \quad (6)$$

with the phase space density F as a function of equatorial pitch angle α_e and momentum p, the EMIC-driven drift-averaged diffusion rates in equatorial pitch angle $\langle D_{\alpha_e\alpha_e}\rangle$, momentum $\langle D_{pp}\rangle$, and cross term $\langle D_{\alpha_e p}\rangle = \langle D_{p\alpha_e}\rangle$, $G = p^2 T(\alpha_e)\sin\alpha_e\cos\alpha_e$ and $T \approx 1.30 - 0.56\sin\alpha_e$. The simulation code is still extracted from our previously developed STEERB model (Su et al., 2010a, 2010b, 2011b). The EMIC wave-driven diffusion is included only in the time range 19:25–21:05 UT of the RBSP-observed dip structure (Figure 2b). It should be mentioned that the spatial locations of intense EMIC waves can vary considerably with time because of the rapid evolution of hot protons and background conditions (Jordanova et al., 2008; Zhang et al., 2014). Due to the limitation of the orbital coverage, the RBSP satellites did not observe the EMIC waves throughout the dip period. The initial condition F_0 is given by the prestorm electron PSD of RBSP-A around 16:08 UT. The boundary conditions are specified as

$$F|_{E_k=0.1\ \mathrm{MeV}} = F_0|_{E_k=0.1\ \mathrm{MeV}}, \quad (7)$$

$$\partial F/\partial p|_{E_k=10.0\ \mathrm{MeV}} = 0, \quad (8)$$

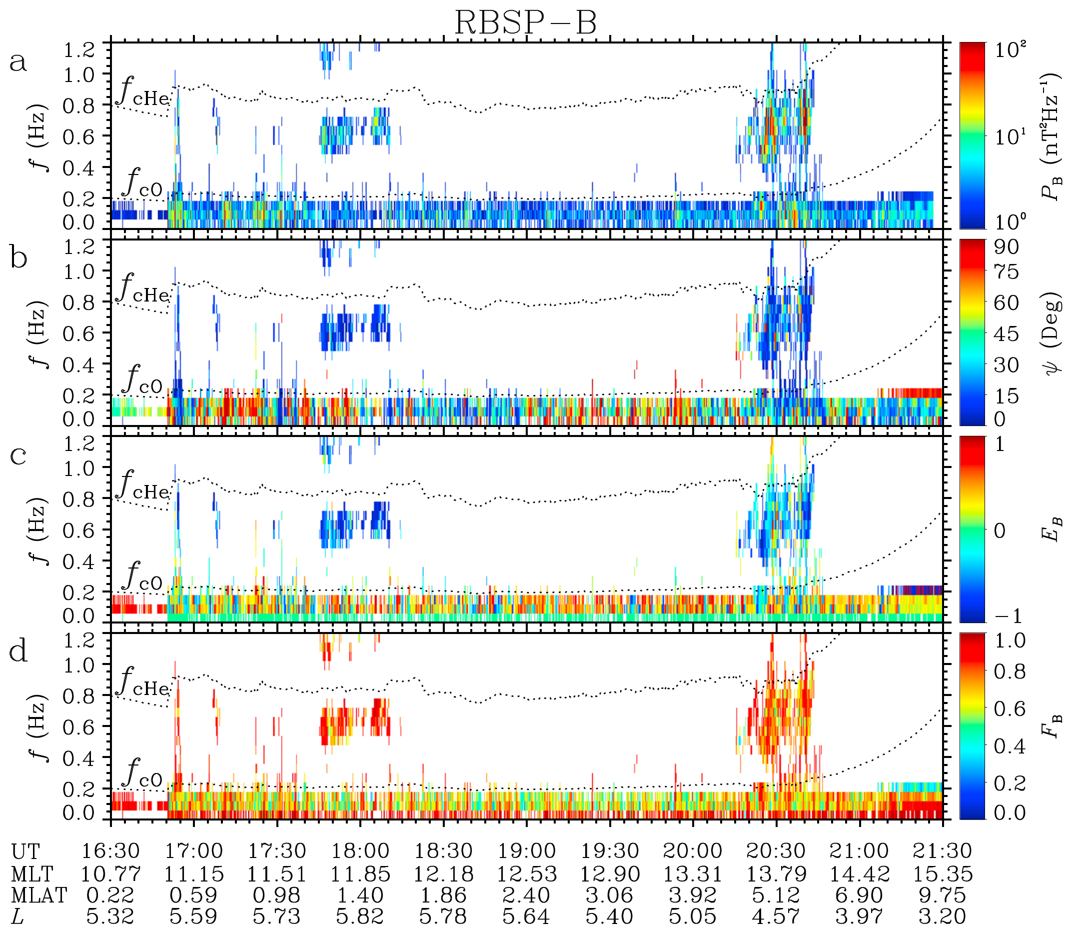

Figure 8. EMIC wave characteristics observed by RBSP-B: (a) magnetic power spectral density P_{B}, (b) normal angle ψ, (c) ellipticity E_{B}, and (d) planarity F_{B}. The dotted lines represent the equatorial gyrofrequencies of helium f_{cHe} and oxygen f_{cO} ions.

$$F|_{\alpha_{\mathrm{e}}=5^\circ} = 0, \tag{9}$$

$$\partial F/\partial \alpha_{\mathrm{e}}|_{\alpha_{\mathrm{e}}=90^\circ} = 0. \tag{10}$$

We use the singular value decomposition (SVD) method (Santolík et al., 2003) to determine the propagation characteristics of EMIC waves observed by twin RBSP (Figures 7 and 8). These waves had high values of planarity (close to 1), allowing the application of SVD method. The corresponding values of ellipticity were close to −1, indicating that these waves were predominantly left-hand circularly polarized. Most of these EMIC waves propagated quasi-parallel to the ambient magnetic field with normal angles below 20°. It has been shown that the parallel and moderately oblique (< 45°) EMIC waves have the approximately same diffusion coefficients (Albert, 2008, Figure 4). Hence, for simplicity, we calculate the diffusion rates of EMIC waves based on the parallel propagation approximation (Albert, 2003; Summers & Thorne, 2003). The wave frequency distribution is obtained by averaging RBSP-A data over 20:12–21:02 UT and RBSP-B data over 20:25–20:42 UT, and the averaged wave frequency distribution is fitted to a Gaussian function (Albert, 2003, 2005)

$$P_{\mathrm{B}} = \frac{2B_{\mathrm{t}}^2}{\pi^{1/2} f_{\mathrm{d}}} \left[\mathrm{erf}\left(\frac{f_2 - f_{\mathrm{m}}}{f_{\mathrm{d}}}\right) + \mathrm{erf}\left(\frac{f_{\mathrm{m}} - f_1}{f_{\mathrm{d}}}\right) \right]^{-1} \exp\left[-\left(\frac{f - f_m}{f_{\mathrm{d}}}\right)^2 \right]. \tag{11}$$

with the lower limit $f_1 = 0.60 f_{\mathrm{cHe}}$, the upper limit $f_2 = 0.98 f_{\mathrm{cHe}}$, the center $f_{\mathrm{m}} = 0.70 f_{\mathrm{cHe}}$, the half width $f_{\mathrm{d}} = 0.20 f_{\mathrm{cHe}}$, and the amplitude $B_{\mathrm{t}} = 1.9$ nT (Figure 9a). As shown in Figures 7 and 8, the intense EMIC waves emerged within a quite limited range of magnetic local time (MLT = 13.13–13.33, and 13.56–13.88 for RBSP-A and MLT = 13.63–13.95 for RBSP-B). We assume that EMIC waves were distributed within 0.48 h of magnetic

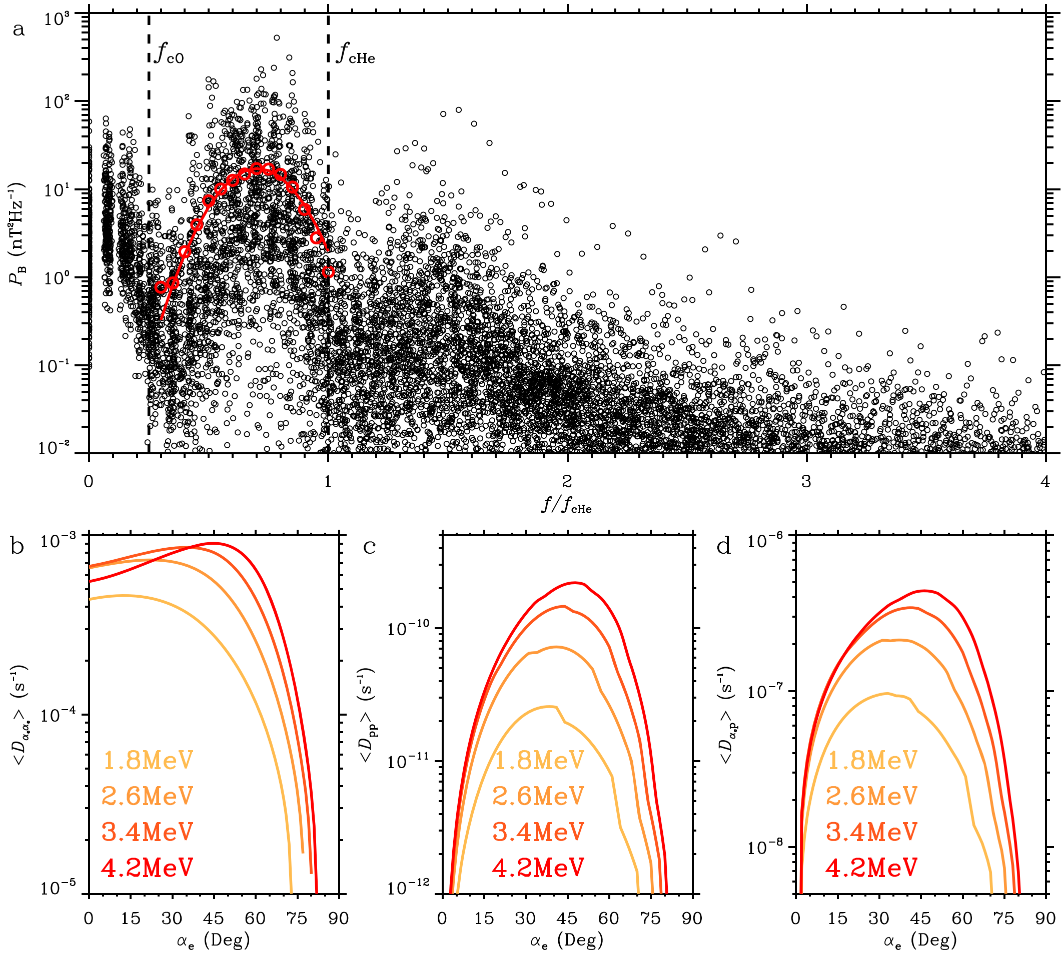

Figure 9. EMIC wave spectra and diffusion rates: (a) EMIC wave spectra P_B directly detected by RBSP (black circles), averaged over time (red circles), and fitted to a Gaussian function (red line); and (b–d) drift-averaged diffusion rates (color coded according to energy) in equatorial pitch angle $\langle D_{\alpha_e\alpha_e} \rangle$, momentum $\langle D_{pp} \rangle$, and cross term $\langle D_{\alpha_e p} \rangle$.

local time. This MLT occurrence ratio 2% is comparable to the simulation parameters 1%–5% in the previous studies (e.g., Summers et al., 2007; Li et al., 2007; Shprits et al., 2009; Su et al., 2011a). Following the early studies (e.g., Summers et al., 2007: Li et al., 2007), we include EMIC waves in the latitudinal range $|\lambda| \leq 15°$. The background ion compositions are specified as 77%H^+ + 20%He^+ + 3%O^+ (typical values during storms) (Jordanova et al., 2008). The equatorial magnetic field at $L = 4.5$ is taken to be B_0 =263 nT on the basis of observations, and the field-aligned magnetic amplitude is set to follow the dipole model. The equatorial ratio between plasma frequency and electron gyrofrequency $f_{pe}/f_{ce} = 22$ is inferred from the measurements of EMFISIS suite (Kurth et al., 2015). The obtained drift-averaged diffusion rates of EMIC waves are plotted in Figure 9. Pitch angle diffusion is found to be absolutely dominant over momentum and cross diffusion, favoring the rapid precipitation loss of relativistic electrons. The evolution of relativistic electrons is predominantly controlled by the pitch angle diffusion of EMIC waves, and the inaccuracy of the lower boundary condition (7) will not significantly affect the relativistic electron dynamics in the simulations. As calculated by Summers and Thorne (2003), the strong diffusion limits for relativistic electrons are above 10^{-2} s^{-1} in the center of the outer radiation belt. The drift-averaged pitch angle diffusion coefficients here are much smaller than the strong diffusion limits, allowing the application of zero boundary condition (9) near the loss cone.

Figure 10a shows the high-density plasmasphere structure modeled by Goldstein et al., (2014) and the EMIC waves observed by twin RBSP. Due to the enhanced magnetospheric convection during the storm, the high-density plasmasphere (gray shadow) was eroded and the plasmaspheric plume formed in the dayside. The twin RBSP trajectories (black lines) were located in the plasmasphere most of the time. The intense

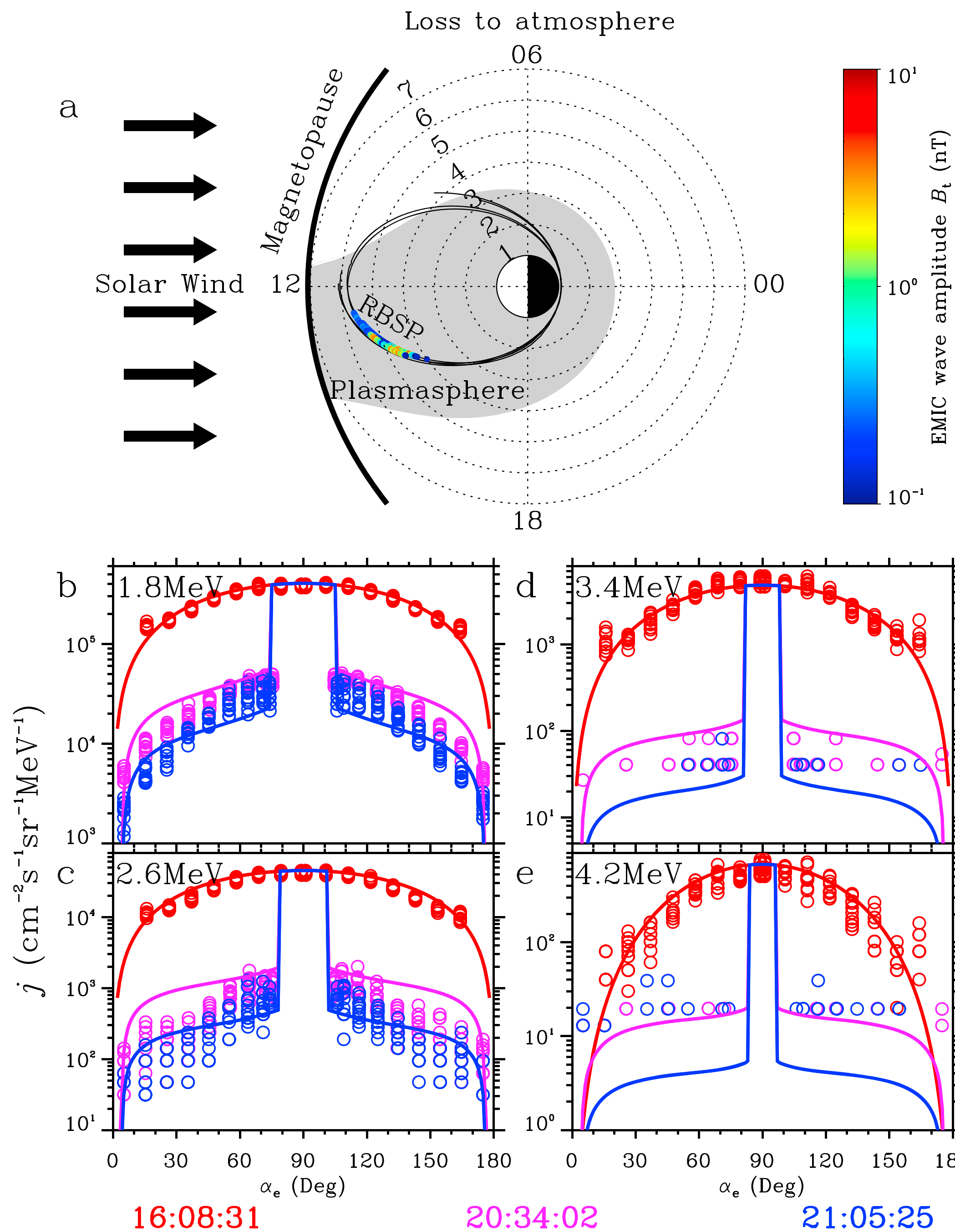

Figure 10. Comparison of observation with simulation of loss to atmosphere: (a) spatial distribution of EMIC waves (color coded according to wave amplitude B_t), with the gray shadow representing the modeled high-density plasmasphere around 20:30 UT (Goldstein et al., 2014); and (b–e) observed (circles) and simulated (lines) equatorial pitch angle distributions $j = p^2 F$ (color coded according to time) of relativistic electrons at the different energy channels (shown) in the heart of the outer radiation belt ($L = 4.5$). In Figures 10b–10e, the observed electron fluxes within a 2 min window have been plotted at each time point.

EMIC waves occurred within a quite limited longitudinal region of the magnetospheric afternoon sector, qualitatively consistent with the previous global simulations (Jordanova et al., 2008, Figure 1).

Figures 10b–10e present the comparison between observed and simulated relativistic electron PADs. The observed local pitch angle α is mapped to the equatorial pitch angle α_e along the TS04-modeled geomagnetic field line. The observed α-dependent PSDs $F(\alpha)$ are directly transformed into the α_e-dependent PSDs

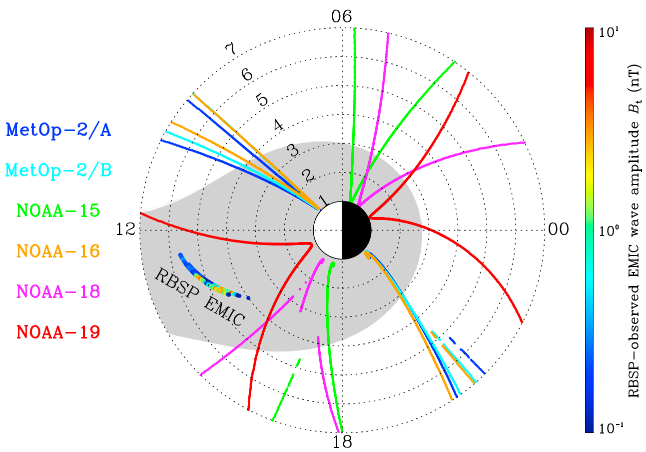

Figure 11. Trajectories of RBSP and POES satellites projected along the magnetic field lines onto the equator. The plotted time range corresponds to the time period of dip structure (19:25–21:05 UT) observed by RBSP satellites (Figure 2). The gray shadow represents the modeled high-density plasmasphere around 20:30 UT (Goldstein et al., 2014). The RBSP trajectories are color coded according to the corresponding EMIC wave amplitude B_t.

$F(\alpha_e) = F\left(\alpha = \arcsin\left(\sin\alpha_e\sqrt{\frac{B_{Mo}}{B_{Me}}}\right)\right)$, with the ratio $\frac{B_{Mo}}{B_{Me}}$ between local B_{Mo} and equatorial B_{Me} magnetic fields in the TS04 model. Note that at the latter two time points, the RBSP located at the magnetic latitude $\lambda \approx 5°$ were unable to measure the fluxes of electrons ($\alpha_e > 80°$) mirroring around the equator. Under the action of EMIC waves within a quite limited longitudinal region, the simulations agree reasonably well with observations for the relativistic electrons mirroring off the equator. As a result of the monotonically increasing diffusion strength with increasing energy (Figure 9), stronger depletion occurs at higher-energy channels. As the electron energy increases, the peak of pitch angle diffusion rate moves toward $\alpha_e = 90°$ (Figure 9). Consequently, the pitch angle distributions in the range $10° < |\alpha_e - 90°| < 80°$ tend to be more flat at higher-energy channels. It should be mentioned that the actual wave properties (e.g., spatial and frequency distributions) and the background conditions (e.g., plasma density and magnetic field) changed considerably with time. To reproduce every detail of the observed electron flux evolution can be quite difficult because of the lack of the accurate time-dependent wave/background parameters. At 1.8 and 2.6 MeV, the model-data difference is comparable to the fluctuation magnitude of the observed electron fluxes within a 2 min window. At 3.4 MeV and 4.2 MeV, the observed electron fluxes were reduced to the noise level, and the modeled scattering by EMIC appears to be sufficient to explain the electron loss magnitude. These results suggest that the EMIC-driven pitch angle scattering was likely to be the dominant loss mechanism in the heart of the outer radiation belt.

The POES system at low altitudes ~800 km (Evans & Greer, 2000) are usually expected to monitor the radiation belt electron precipitation (Horne et al., 2009; Turner et al., 2012; Zhang, Halford, et al., 2016).

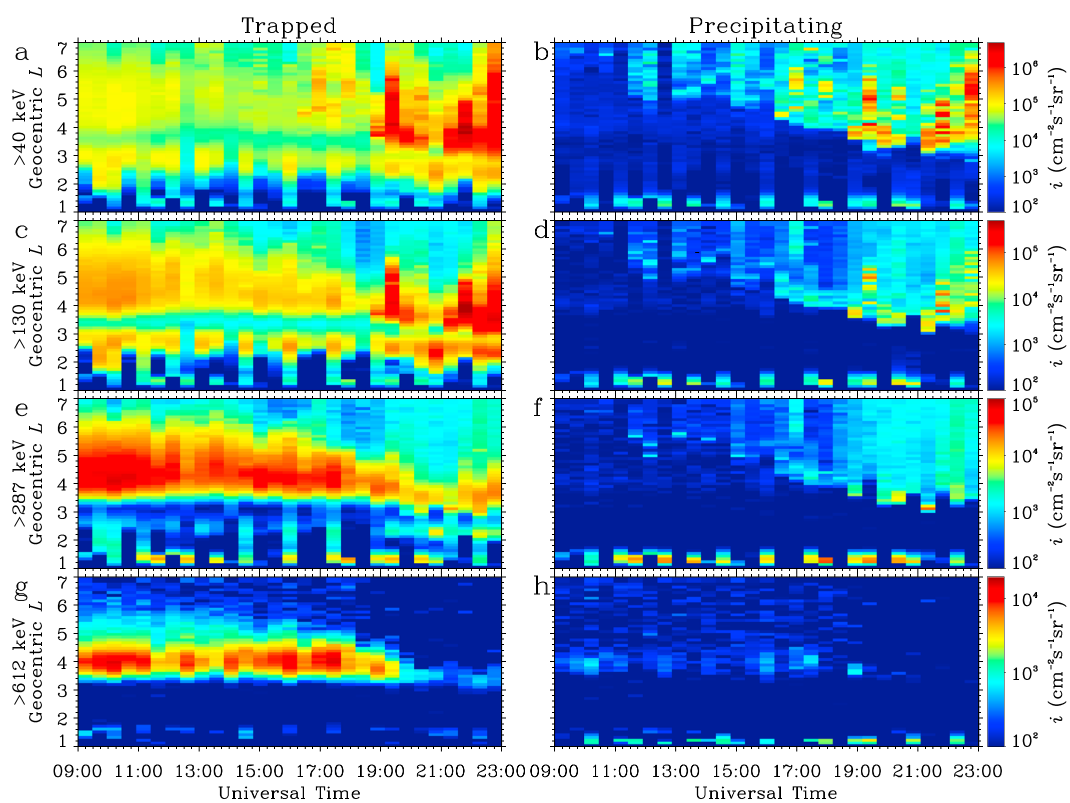

Figure 12. POES-observed evolution of (a, c, e, and g) trapped and (b, d, f, and h) precipitating electrons in the different energy ranges (shown).

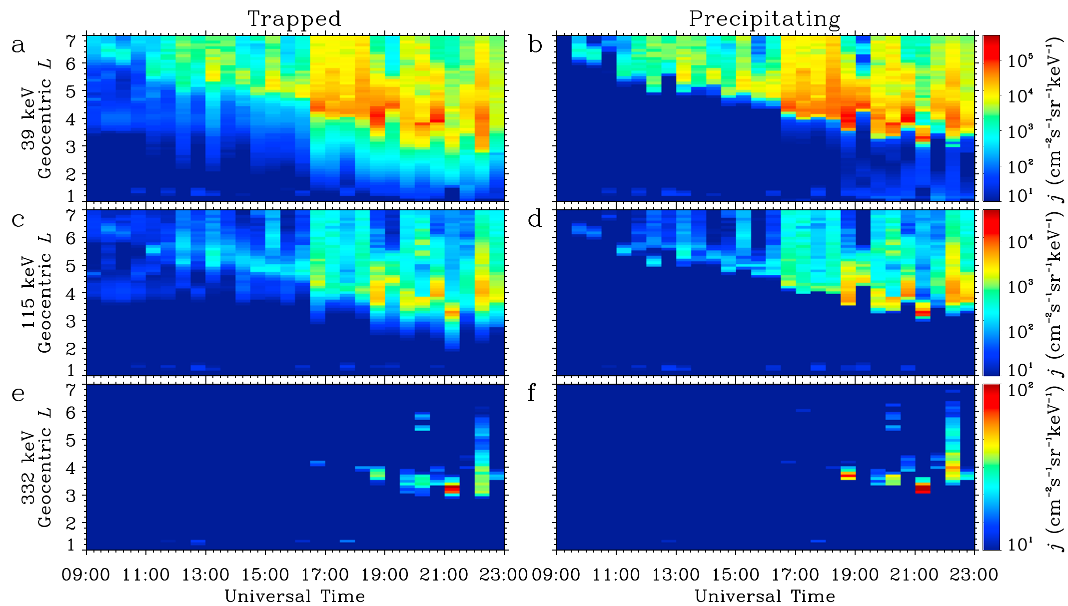

Figure 13. POES-observed evolution of (a, c, and e) trapped and (b, d, and f) precipitating protons at the different energy channels (shown).

On 27 February 2014, data of six POES satellites (MetOp-2/A, MetOp-2/B, NOAA 15, NOAA 16, NOAA18, and NOAA 19) were available (Figure 11). Unfortunately, during the short time period (19:25–21:05 UT) of the flux dip structure observed by twin RBSP (Figure 2b), none of POES satellites passed though the magnetic local time region 1300–1400 with intense EMIC waves. As a result, the POES system cannot detect the particle precipitation induced by EMIC waves in this event (Zhang, Li, et al., 2016). Figure 12 shows the evolution of trapped and precipitating electrons at low altitudes. The enhanced precipitation of electrons occurred primarily at the low energies (40–300 keV, below the minimum resonant energy of typical EMIC waves (Meredith, Thorne, et al., 2003). Figure 13 additionally presents the evolution of protons at low altitudes.

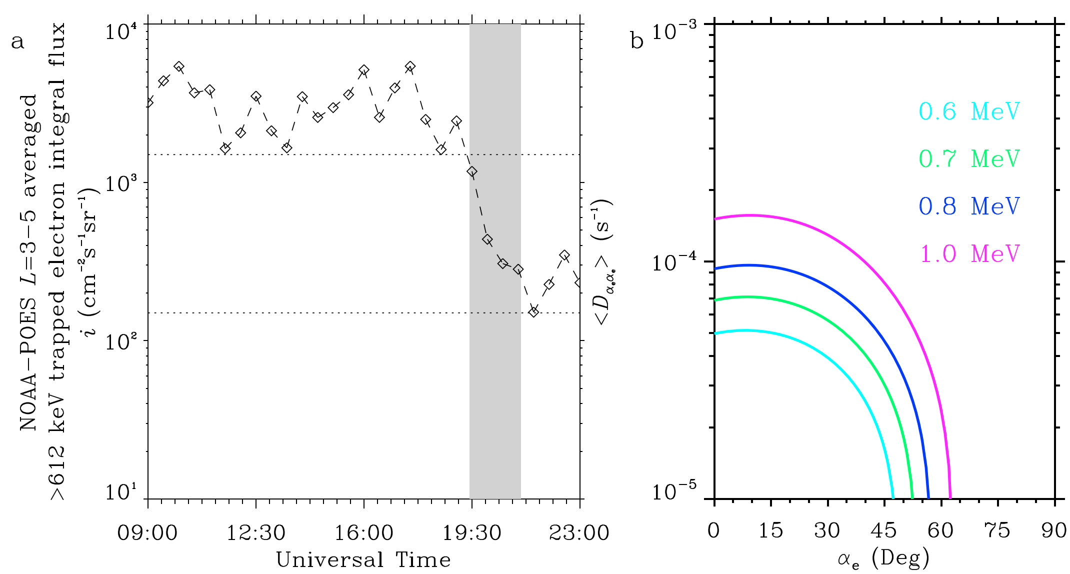

Figure 14. Loss of high-energy trapped electrons at low altitudes: (a) temporal profiles (squares) of the NOAA-POES observed integral fluxes *i* of >612 keV trapped electrons averaged over the core part of the outer radiation belt (L = 3–5) and (b) drift-averaged pitch angle diffusion rates by EMIC waves (color coded according to energy). In Figure 14a, the dashed lines are introduced to guide the eye; the dotted lines are overplotted to help identify the electron flux variation; the gray shadow marks the time period of dip structure (19:25–21:05 UT) observed by twin RBSP (Figure 2b).

There was a clear correspondence between enhancements in the trapped and precipitating proton fluxes, but no observable sign for the proton precipitations is related to EMIC waves (Bortnik et al., 2006). However, benefiting from the operations of multiple satellites and their short orbital periods (∼100 min), the POES system can monitor the radial profiles of radiation belt with a high time resolution. We average the relativistic (>612 keV) electron integral fluxes over the core part ($L = 3-5$) of the outer radiation belt with a time resolution of 0.5 h (Figure 14a). At energies >600 keV, the efficient pitch angle diffusion by EMIC waves can still act over the pitch angles <30° (Figure 14b). These trapped electrons were lost predominantly in the time period 19:25–21:05 UT during which the dip structure of relativistic electron fluxes was observed by twin RBSP at low latitudes. Outside this time period, no significant loss of trapped electrons can be identified. These data demonstrate once again that the loss of high-energy electrons in the heart of the outer radiation belt was not caused primarily by the ULF wave-driven outward radial diffusion starting around 17:00 UT but rather by the EMIC wave driven pitch angle scattering starting around 19:25 UT.

5. Conclusion and Discussion

There have been two main competing paradigms for the loss of radiation belt relativistic electrons: radial loss to the magnetopause (Shprits, Thorne, Friedel, et al., 2006; Loto'Aniu et al., 2010) and local loss to the atmosphere (Thorne & Kennel, 1971; Horne & Thorne, 1998; Summers et al., 1998). For the former, the primary observational evidence is the radially peaked PSD profile of relativistic electrons (Turner et al., 2012; Mann et al., 2016); for the latter, the observational evidences frequently mentioned in previous works are the wave-related electron precipitation at low altitudes (Lorentzen et al., 2001; Millan et al., 2002; Miyoshi et al., 2008; Tsurutani et al., 2013; Breneman et al., 2015) and the flat-top PAD characteristic (Usanova et al., 2014; Engebretson et al., 2015; Su et al., 2016; Shprits et al., 2016). Here on the basis of the analysis of an extreme radiation belt electron loss event observed by RBSP and POES on 27 February 2014, we present new evidence for the EMIC wave-driven local precipitation loss of relativistic electrons in the heart of the outer radiation belt:

1. The RBSP-observed radial profile of the relativistic electron PSD appeared to be quasi-monotonic, in contrast to the peaked type of previously reported events (e.g., Turner et al., 2014; Mann et al., 2016). Although the radial loss indeed occurred at high L shells, the local loss should act at low L shells to prevent the development of PSD peak. As far as we know, this is the first report of the evidence for the dominance of local loss from the perspective of PSD radial characteristic. Such an evidence is parallel to the frequently mentioned evidence (peaked PSD characteristic) for the action of local acceleration in the outer radiation belt (e.g., Green and Kivelson 2004; Chen et al., 2007; Reeves et al., 2013).
2. The RBSP-observed temporal profile of the relativistic electron flux exhibited a clear dip with an evident correspondence to intense EMIC waves in the heart of the outer radiation belt. Such an evidence for the EMIC-driven loss was rarely reported in the past due to the lack of observations with high resolution in both space and time. Unfortunately, none of POES satellites passed though the magnetic local time region 1300–1400 with intense EMIC waves. Consequently, the POES system did not capture the precipitation of relativistic electrons. However, the POES observations did show that the relativistic electrons trapped in the heart of the outer radiation belt were lost primarily during the time period of the dip structure. Our simulations quantitatively confirm that the observed EMIC waves within a quite limited longitudinal region can reduce the off-equatorially mirroring relativistic electron fluxes by up to 2 orders of magnitude within about 1.5 h.

The whistler mode plasmaspheric hiss (Horne & Thorne, 1998; Summers et al., 1998; Breneman et al., 2015) and magnetosonic waves (Roberts & Schulz 1968, Shprits; 2009) may also contribute to the local precipitation loss of relativistic electrons. As shown in the previous simulations (e.g., Li et al., 2007; Su et al., 2016), the typical loss time scale of the off-equatorially mirroring relativistic electrons driven by plasmaspheric hiss waves (a few days to hundreds of days) is much larger than that associated with EMIC waves (hours) (e.g., Summers et al., 2007, 2008). For the near-equatorially trapped electrons, the scattering of plasmaspheric hiss would become dominant. However, as shown in Figure 15, the spatiotemporal characteristics of plasmaspheric hiss appeared to be quite complicated. Although the twin RBSP were always located in the high-density plasmasphere (with the upper hybrid resonance frequency measured by the high-frequency receiver (Kurth et al., 2015) of the EMFISIS Waves instrument above 40 kHz in Figures 15b and 15d), the hiss waves (measured by the waveform receiver of the EMFISIS Waves instrument in Figures 15c and 15e) disappeared abruptly

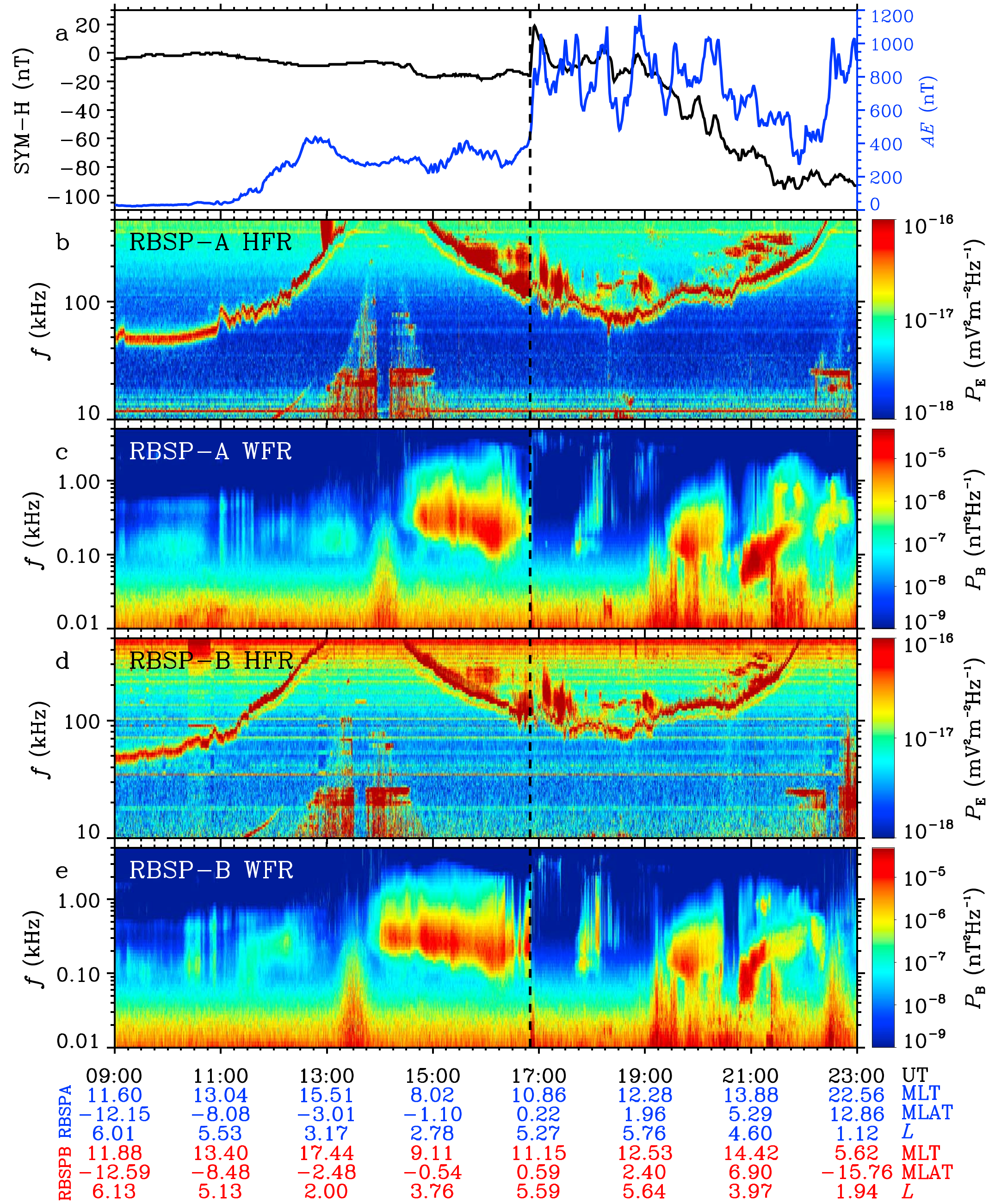

Figure 15. An overview of geospace environment on 27 February 2014: (a) geomagnetic activity indices *SYM-H* and *AE* and (b–e) wave electric/magnetic power spectral densities (color coded). The vertical dashed line marks the arrival of the interplanetary shock. In Figures 15b and 15d, the bright line corresponds to the upper hybrid resonance frequency line (Kurth et al., 2015).

following the interplanetary shock (similar to the events reported by Su, Zhu, Xiao, Zheng, et al., 2015 and Liu et al., 2017) and recovered intermittently in the next several hours. It is hard to determine the global distribution of plasmaspheric hiss waves on the basis of available data in this event. Through the bounce resonance (Roberts & Schulz, 1968; Shprits, 2009), the magnetosonic waves can scatter the equatorially trapped electrons toward the lower pitch angles. For this specific event, the intense magnetosonic waves were not observed by the RBSP, and consequently, their spatiotemporal and spectral characteristics remained unclear. Meanwhile, the measurements of near-equatorially trapped electrons were not available most of the time (Figure 10) due to the limitation of RBSP orbits in this event. Hence, the contributions of plasmaspheric hiss and magnetosonic waves to the loss of radiation belt electrons are not quantified in this study.

In this study, we concentrate on the loss of approximately greater than MeV electrons in the heart of the outer radiation belt. At lower energy channels (hundreds of keV), there was only a ∼<8 times reduction of the electron fluxes and the so-called dip structure became insignificant. It is well known that the loss efficiency of EMIC waves decreases rapidly with the electron energy decreasing (e.g., Summers et al., 2007). The loss of hundreds of keV electrons might result from a subtle combination of the radial diffusion by ULF waves and the pitch angle scattering by plasmaspheric hiss and EMIC waves (e.g., Su et al., 2016). However, because of the limitation of the orbital coverage of RBSP and the complicated evolution of plasmaspheric hiss and ULF waves in this event, it is difficult to differentiate among the contributions of the three types of waves in the loss of hundreds of keV electrons.

Acknowledgments
This work was supported by the National Natural Science Foundation of China grants 41422405, 41631071, 41774170, 41274169, 41274174, 41174125, 41131065, 41421063, 41231066, and 41304134, the Chinese Academy of Sciences grant KZCX2-EW-QN510 and KZZD-EW-01-4, the CAS Key Research Program of Frontier Sciences grant QYZDB-SSW-DQC015, the National Key Basic Research Special Foundation of China grant 2011CB811403, and the Fundamental Research Funds for the Central Universities WK2080000077. We acknowledge the University of Iowa as the source for the EMFISIS data (this acknowledgement does not imply endorsement of the publication by the University of Iowa or its researchers). The data are available at the websites: RBSP-EMFSIS: http://emfisis.physics.uiowa.edu/Flight/, RBSP-ECT: http://www.rbsp-ect.lanl.gov/data_pub/, and POES: https://cdaweb.sci.gsfc.nasa.gov/index.html/.

References

Albert, J. (2014). Radial diffusion simulations of the 20 September 2007 radiation belt dropout. *Annales Geophysicae*, *32*, 925–934. https://doi.org/10.5194/angeo-32-925-2014

Albert, J. M. (2003). Evaluation of quasi-linear diffusion coefficients for EMIC waves in a multispecies plasma. *Journal of Geophysical Research*, *108*(A8), 1249. https://doi.org/10.1029/2002JA009792

Albert, J. M. (2005). Evaluation of quasi-linear diffusion coefficients for whistler mode waves in a plasma with arbitrary density ratio. *Journal of Geophysical Research*, *110*, A03218. https://doi.org/10.1029/2004JA010844

Albert, J. M. (2008). Efficient approximations of quasi-linear diffusion coefficients in the radiation belts. *Journal of Geophysical Research*, *113*, A06208. https://doi.org/10.1029/2007JA012936

Anderson, B., Millan, R., Reeves, G. D., & Friedel, R. H. W. (2015). Acceleration and loss of relativistic electrons during small geomagnetic storms. *Geophysical Research Letters*, *42*, 10,113–10,119. https://doi.org/10.1002/2015GL066376

Baker, D. N., Kanekal, S. G., Hoxie, V. C., Batiste, S., Bolton, M., Li, X., … Friedel, R. (2013). The Relativistic Electron-Proton Telescope (REPT) instrument on board the Radiation Belt Storm Probes (RBSP) spacecraft: Characterization of Earth's radiation belt high-energy particle populations. *Space Science Reviews*, *179*, 337–381. https://doi.org/10.1007/s11214-012-9950-9

Baker, D. N., Klebesadel, R. W., Higbie, P. R., & Blake, J. B. (1986). Highly relativistic electrons in the Earth's outer magnetosphere. I—Lifetimes and temporal history 1979–1984. *Journal of Geophysical Research*, *91*, 4265–4276. https://doi.org/10.1029/JA091iA04p04265

Bortnik, J., Thorne, R. M., O'Brien, T. P., Green, J. C., Strangeway, R. J., Shprits, Y. Y., & Baker, D. N. (2006). Observation of two distinct, rapid loss mechanisms during the 20 November 2003 radiation belt dropout event. *Journal of Geophysical Research*, *111*, A12216. https://doi.org/10.1029/2006JA011802

Brautigam, D. H., & Albert, J. M. (2000). Radial diffusion analysis of outer radiation belt electrons during the October 9, 1990, magnetic storm. *Journal of Geophysical Research*, *105*, 291–310. https://doi.org/10.1029/1999JA900344

Breneman, A., Halford, A., Millan, R., McCarthy, M., Fennell, J., Sample, J., … Kletzing, C. (2015). Global-scale coherence modulation of radiation-belt electron loss from plasmaspheric hiss. *Nature*, *523*, 193–195. https://doi.org/10.1038/nature14515

Chen, Y., Reeves, G. D., & Friedel, R. H. W. (2007). The energization of relativistic electrons in the outer Van Allen radiation belt. *Nature Physics*, *3*, 614–617. https://doi.org/10.1038/nphys655

Elkington, S. R., Hudson, M. K., & Chan, A. A. (1999). Acceleration of relativistic electrons via drift-resonant interaction with toroidal-mode Pc-5 ULF oscillations. *Geophysical Research Letters*, *26*, 3273–3276. https://doi.org/10.1029/1999GL003659

Engebretson, M. J., Posch, J. L., Wygant, J. R., Kletzing, C. A., Lessard, M. R., Huang, C.-L., … Shiokawa, K. (2015). Van Allen probes, NOAA, GOES, and ground observations of an intense EMIC wave event extending over 12 h in magnetic local time. *Journal of Geophysical Research: Space Physics*, *120*, 5465–5488. https://doi.org/10.1002/2015JA021227

Evans, D. S., & Greer, M. S. (2000). *Polar Orbiting Environmental Satellite Space Environment Monitor-2: Instrument Description and Archive Data Documentation*: US Department of Commerce, National Oceanic and Atmospheric Administration, Oceanic and Atmospheric Research Laboratories, Space Environment Center. Boulder, CO.

Friedel, R. H. W., Reeves, G. D., & Obara, T. (2002). Relativistic electron dynamics in the inner magnetosphere—A review. *Journal of Atmospheric and Solar-Terrestrial Physics*, *64*, 265–282. https://doi.org/10.1016/S1364-6826(01) 00088-8

Gao, Z., Su, Z., Zhu, H., Xiao, F., Zheng, H., Wang, Y., … Wang, S. (2016). Intense low-frequency chorus waves observed by Van Allen Probes: Fine structures and potential effect on radiation belt electrons. *Geophysical Research Letters*, *43*, 967–977. https://doi.org/10.1002/2016GL067687

Goldstein, J., Pascuale, S. D., Kletzing, C., Kurth, W., Genestreti, K. J., Skoug, R. M., … Spence, H. (2014). Simulation of Van Allen Probes plasmapause encounters. *Journal of Geophysical Research: Space Physics*, *119*, 7464–7484. https://doi.org/10.1002/2014JA020252

Green, J. C., & Kivelson, M. G. (2004). Relativistic electrons in the outer radiation belt: Differentiating between acceleration mechanisms. *Journal of Geophysical Research*, *109*, A03213. https://doi.org/10.1029/2003JA010153

Horne, R. B., & Thorne, R. M. (1998). Potential waves for relativistic electron scattering and stochastic acceleration during magnetic storms. *Geophysical Research Letters*, *25*, 3011–3014. https://doi.org/10.1029/98GL01002

Horne, R. B., Lam, M. M., & Green, J. C. (2009). Energetic electron precipitation from the outer radiation belt during geomagnetic storms. *Geophysical Research Letters*, *36*, L19104. https://doi.org/10.1029/2009GL040236

Horne, R. B., Meredith, N. P., Thorne, R. M., Heynderickx, D., Iles, R. H. A., & Anderson, R. R. (2003). Evolution of energetic electron pitch angle distributions during storm time electron acceleration to megaelectronvolt energies. *Journal of Geophysical Research*, *108*(A1), 1016. https://doi.org/10.1029/2001JA009165

Horne, R. B., Thorne, R. M., Glauert, S. A., Albert, J. M., Meredith, N. P., & Anderson, R. R. (2005). Timescale for radiation belt electron acceleration by whistler mode chorus waves. *Journal of Geophysical Research*, *110*, A03225. https://doi.org/10.1029/2004JA010811

Horne, R. B., Thorne, R. M., Shprits, Y. Y., Meredith, N. P., Glauert, S. A., Smith, A. J., … Decreau, P. M. E. (2005). Wave acceleration of electrons in the Van Allen radiation belts. *Nature*, *437*, 227–230. https://doi.org/10.1038/nature03939

Hudson, M. K., Baker, D. N., Goldstein, J., Kress, B. T., Paral, J., Toffoletto, F. R., & Wiltberger, M. (2014). Simulated magnetopause losses and Van Allen Probe flux dropouts. *Geophysical Research Letters*, *41*, 1113–1118. https://doi.org/10.1002/2014GL059222

Jordanova, V. K., Albert, J., & Miyoshi, Y. (2008). Relativistic electron precipitation by EMIC waves from self-consistent global simulations. *Journal of Geophysical Research*, *113*, A00A10. https://doi.org/10.1029/2008JA013239

Kletzing, C. A., Kurth, W. S., Acuna, M., MacDowall, R. J., Torbert, R. B., Averkamp, T., … Tyler, J. (2013). The Electric and Magnetic Field Instrument Suite and Integrated Science (EMFISIS) on RBSP (EMFISIS) on RBSP. *Space Science Reviews*, *179*, 127–181. https://doi.org/10.1007/s11214-013-9993-6

Kurth, W. S., De Pascuale, S., Faden, J. B., Kletzing, C. A., Hospodarsky, G. B., Thaller, S., & Wygant, J. R. (2015). Electron densities inferred from plasma wave spectra obtained by the Waves instrument on Van Allen Probes. *Journal of Geophysical Research*, *120*, 904–914. https://doi.org/10.1002/2014JA020857

Li, W., Shprits, Y. Y., & Thorne, R. M. (2007). Dynamic evolution of energetic outer zone electrons due to wave-particle interactions during storms. *Journal of Geophysical Research*, *112*, A10220. https://doi.org/10.1029/2007JA012368

Li, X., Baker, D. N., Temerin, M., Cayton, T. E., Reeves, E. G. D., Christensen, R. A., … Kanekal, S. G. (1997). Multisatellite observations of the outer zone electron variation during the November 3–4, 1993, magnetic storm. *Journal of Geophysical Research*, *102*, 14,123–14,140. https://doi.org/10.1029/97JA01101

Liu, N., Su, Z., Gao, Z., Zheng, H., Wang, Y., Wang, S., … Wygant, J. R. (2017). Simultaneous disappearances of plasmaspheric hiss, exohiss, and chorus waves triggered by a sudden decrease in solar wind dynamic pressure. *Geophysical Research Letters*, *44*, 52–61. https://doi.org/10.1002/2016GL071987

Lorentzen, K. R., Blake, J. B., Inan, U. S., & Bortnik, J. (2001). Observations of relativistic electron microbursts in association with VLF chorus. *Journal of Geophysical Research*, *106*, 6017–6028. https://doi.org/10.1029/2000JA003018

Loto'Aniu, T. M., Mann, I. R., Ozeke, L. G., Chan, A. A., Dent, Z. C., & Milling, D. K. (2006). Radial diffusion of relativistic electrons into the radiation belt slot region during the 2003 Halloween geomagnetic storms. *Journal of Geophysical Research*, *111*, A04218. https://doi.org/10.1029/2005JA011355

Loto'Aniu, T. M., Singer, H. J., Waters, C. L., Angelopoulos, V., Mann, I. R., Elkington, S. R., & Bonnell, J. W. (2010). Relativistic electron loss due to ultralow frequency waves and enhanced outward radial diffusion. *Journal of Geophysical Research*, *115*, A12245. https://doi.org/10.1029/2010JA015755

Lyons, L. R., & Williams, D. J. (1984). *Quantitative aspects of magnetospheric physics*. Springer: New York.

Mann, I., Ozeke, L., Murphy, K., Claudepierre, S., Turner, D., Baker, D., … Honary, F. (2016). Explaining the dynamics of the ultra-relativistic third Van Allen radiation belt. *Nature Physics*, *12*, 978–983. https://doi.org/10.1038/NPHYS3799

Mathie, R. A., & Mann, I. R. (2000). A correlation between extended intervals of ULF wave power and storm-time geosynchronous relativistic electron flux enhancements. *Geophysical Research Letters*, *27*, 3261–3264. https://doi.org/10.1029/2000GL003822

Mauk, B. H., Fox, N. J., Kanekal, S. G., Kessel, R. L., Sibeck, D. G., & Ukhorskiy, A. (2013). Science objectives and rationale for the radiation belt storm probes mission. *Space Science Reviews*, *179*, 3–27. https://doi.org/10.1007/s11214-012-9908-y

Meredith, N. P., Cain, M., Horne, R. B., Thorne, R. M., Summers, D., & Anderson, R. R. (2003). Evidence for chorus-driven electron acceleration to relativistic energies from a survey of geomagnetically disturbed periods. *Journal of Geophysical Research*, *108*, 1248. https://doi.org/10.1029/2002JA009764

Meredith, N. P., Thorne, R. M., Horne, R. B., Summers, D., Fraser, B. J., & Anderson, R. R. (2003). Statistical analysis of relativistic electron energies for cyclotron resonance with EMIC waves observed on CRRES. *Journal of Geophysical Research*, *108*, 1250. https://doi.org/10.1029/2002JA009700

Millan, R. M., & Thorne, R. M. (2007). Review of radiation belt relativistic electron losses. *Journal of Atmospheric and Solar-Terrestrial Physics*, *69*, 362–377. https://doi.org/10.1016/j.jastp.2006.06.019

Millan, R. M., Lin, R. P., Smith, D. M., Lorentzen, K. R., & McCarthy, M. P. (2002). X-ray observations of MeV electron precipitation with a balloon-borne germanium spectrometer. *Geophysical Research Letters*, *29*(24), 2194. https://doi.org/10.1029/2002GL015922

Miyoshi, Y., Sakaguchi, K., Shiokawa, K., Evans, D., Albert, J., Connors, M., & Jordanova, V. (2008). Precipitation of radiation belt electrons by EMIC waves, observed from ground and space. *Geophysical Research Letters*, *35*, L23101. https://doi.org/10.1029/2008GL035727

Mourenas, D., Artemyev, A. V., Ma, Q., Agapitov, O. V., & Li, W. (2016). Fast dropouts of multi-MeV electrons due to combined effects of EMIC and whistler mode waves. *Geophysical Research Letters*, *43*, 4155–4163. https://doi.org/10.1002/2016GL068921

Ni, B., Li, W., Thorne, R. M., Bortnik, J., Ma, Q., Chen, L., … Claudepierre, S. G. (2014). Resonant scattering of energetic electrons by unusual low-frequency hiss. *Geophysical Research Letters*, *41*, 1854–1861. https://doi.org/10.1002/2014GL059389

Omura, Y., Miyashita, Y., Yoshikawa, M., Summers, D., Hikishima, M., Ebihara, Y., & Kubota, Y. (2015). Formation process of relativistic electron flux through interaction with chorus emissions in the Earth's innermagnetosphere. *Journal of Geophysical Research: Space Physics*, *120*, 9545–9562. https://doi.org/10.1002/2015JA021563

Onsager, T. G., Rostoker, G., Kim, H.-J., Reeves, G. D., Obara, T., Singer, H. J., & Smithtro, C. (2002). Radiation belt electron flux dropouts: Local time, radial, and particle-energy dependence. *Journal of Geophysical Research*, *107*, 1382. https://doi.org/10.1029/2001JA000187

Ozeke, L. G., Mann, I. R., Murphy, K. R., Jonathan Rae, I., & Milling, D. K. (2014). Analytic expressions for ULF wave radiation belt radial diffusion coefficients. *Journal of Geophysical Research: Space Physics*, *119*, 1587–1605. https://doi.org/10.1002/2013JA019204

Reeves, G. D., Friedel, R. H. W., Larsen, B. A., Skoug, R. M., Funsten, H. O., Claudepierre, S. G., … Baker, D. N. (2016). Energy-dependent dynamics of keV to MeV electrons in the inner zone, outer zone, and slot regions. *Journal of Geophysical Research: Space Physics*, *121*, 397–412. https://doi.org/10.1002/2015JA021569

Reeves, G. D., McAdams, K. L., Friedel, R. H. W., & O'Brien, T. P. (2003). Acceleration and loss of relativistic electrons during geomagnetic storms. *Geophysical Research Letters*, *30*, 1529. https://doi.org/10.1029/2002GL016513

Reeves, G. D., Spence, H. E., Henderson, M. G., Morley, S. K., Friedel, R. H. W., Funsten, H. O., … Niehof, J. T. (2013). Electron acceleration in the heart of the Van Allen radiation belts. *Science*, *341*(6149), 991–994. https://doi.org/10.1126/science.1237743

Roberts, C. S., & Schulz, M. (1968). Bounce resonant scattering of particles trapped in the Earth's magnetic field. *Journal of Geophysical Research*, *73*, 7361–7376. https://doi.org/10.1029/JA073i023p07361

Rostoker, G., Skone, S., & Baker, D. N. (1998). On the origin of relativistic electrons in the magnetosphere associated with some geomagnetic storms. *Geophysical Research Letters*, *25*, 3701–3704. https://doi.org/10.1029/98GL02801

Santolík, O., Parrot, M., & Lefeuvre, F. (2003). Singular value decomposition methods for wave propagation analysis. *Radio Science*, *38*, 1010. https://doi.org/10.1029/2000RS002523

Schiller, Q., Li, X., Blum, L., Tu, W., Turner, D. L., & Blake, J. B. (2014). A nonstorm time enhancement of relativistic electrons in the outer radiation belt. *Geophysical Research Letters*, *41*, 7–12. https://doi.org/10.1002/2013GL058485

Schulz, M., & Lanzerotti, L. J. (1974). Particle diffusion in the radiation belts, *Physics and Chemistry in Space* (Vol. 7, pp. 81–95). New York: Springer-Verlag.

Shprits, Y. Y. (2009). Potential waves for pitch-angle scattering of near-equatorially mirroring energetic electrons due to the violation of the second adiabatic invariant. *Geophysical Research Letters*, *36*, L12106. https://doi.org/10.1029/2009GL038322

Shprits, Y. Y., Chen, L., & Thorne, R. M. (2009). Simulations of pitch angle scattering of relativistic electrons with MLT-dependent diffusion coefficients. *Journal of Geophysical Research*, *114*, A03219. https://doi.org/10.1029/2008JA013695

Shprits, Y. Y., Drozdov, A. Y., Spasojevic, M., Kellerman, A. C., Usanova, M. E., Engebretson, M. J., … Aseev, N. A. (2016). Wave-induced loss of ultra-relativistic electrons in the Van Allen radiation belts. *Nature Communications*, *7*, 12883. https://doi.org/10.1038/ncomms12883

Shprits, Y. Y., Thorne, R. M., Friedel, R., Reeves, G. D., Fennell, J., Baker, D. N., & Kanekal, S. G. (2006). Outward radial diffusion driven by losses at magnetopause. *Journal of Geophysical Research*, *111*, A11214. https://doi.org/10.1029/2006JA011657

Shprits, Y. Y., Thorne, R. M., Horne, R. B., Glauert, S. A., Cartwright, M., Russell, C. T., … Kanekal, S. G. (2006). Acceleration mechanism responsible for the formation of the new radiation belt during the 2003 halloween solar storm. *Geophysical Research Letters*, *33*, L05104. https://doi.org/10.1029/2005GL024256

Shue, J., Song, P., Russell, C. T., Steinberg, J. T., Chao, J. K., Zastenker, G., … Kawano, H. (1998). Magnetopause location under extreme solar wind conditions. *Journal of Geophysical Research*, *103*, 17,691–17,700. https://doi.org/10.1029/98JA01103

Spence, H. E., Reeves, G. D., Baker, D. N., Blake, J. B., Bolton, M., Bourdarie, S., … Thorne, R. M. (2013). Science goals and overview of the Energetic Particle, Composition, and Thermal Plasma (ECT) suite on NASA's Radiation Belt Storm Probes (RBSP) mission. *Space Science Reviews*, *179*, 311–336. https://doi.org/10.1007/s11214-013-0007-5

Su, Z., Xiao, F., Zheng, H., & Wang, S. (2010a). STEERB: A three-dimensional code for storm-time evolution of electron radiation belt. *Journal of Geophysical Research*, *115*, A09208. https://doi.org/10.1029/2009JA015210

Su, Z., Xiao, F., Zheng, H., & Wang, S. (2010b). Combined radial diffusion and adiabatic transport of radiation belt electrons with arbitrary pitch-angles. *Journal of Geophysical Research*, *115*, A10249. https://doi.org/10.1029/2010JA015903

Su, Z., Xiao, F., Zheng, H., & Wang, S. (2011a). CRRES observation and STEERB simulation of the 9 October 1990 electron radiation belt dropout event. *Geophysical Research Letters*, *38*, L06106. https://doi.org/10.1029/2011GL046873

Su, Z., Xiao, F., Zheng, H., & Wang, S. (2011b). Radiation belt electron dynamics driven by adiabatic transport, radial diffusion, and wave-particle interactions. *Journal of Geophysical Research*, *116*, A04205. https://doi.org/10.1029/2010JA016228

Su, Z., Zhu, H., Xiao, F., Zheng, H., Shen, C., Wang, Y., & Wang, S. (2012). Bounce-averaged advection and diffusion coefficients for monochromatic electromagnetic ion cyclotron wave: Comparison between test-particle and quasi-linear models. *Journal of Geophysical Research*, *117*, A09222. https://doi.org/10.1029/2012JA017917

Su, Z., Zhu, H., Xiao, F., Zheng, H., Shen, C., Wang, Y., & Wang, S. (2013). Latitudinal dependence of nonlinear interaction between electromagnetic ion cyclotron wave and radiation belt relativistic electrons. *Journal of Geophysical Research*, *118*, 3188–3202. https://doi.org/10.1002/jgra.50289

Su, Z., Xiao, F., Zheng, H., He, Z., Zhu, H., Zhang, M., … Baker, D. N. (2014). Nonstorm time dynamics of electron radiation belts observed by the Van Allen Probes. *Geophysical Research Letters*, *41*, 229–235. https://doi.org/10.1002/2013GL058912

Su, Z., Zhu, H., Xiao, F., Zong, Q.-G., Zhou, X.-Z., Zheng, H., … Wygant, J. (2015). Ultra-low-frequency wave-driven diffusion of radiation belt relativistic electrons. *Nature Communications*, *6*, 10096. https://doi.org/10.1038/ncomms10096

Su, Z., Zhu, H., Xiao, F., Zheng, H., Wang, Y., Shen, C., … Wygant, J. R. (2015). Disappearance of plasmaspheric hiss following interplanetary shock. *Geophysical Research Letters*, *42*, 3129–3140. https://doi.org/10.1002/2015GL063906

Su, Z., Gao, Z., Zhu, H., Li, W., Zheng, H., Wang, Y., … Wygant, J. R. (2016). Nonstorm time dropout of radiation belt electron fluxes on 24 September 2013. *Journal of Geophysical Research: Space Physics*, *121*, 6400–6416. https://doi.org/10.1002/2016JA022546

Summers, D., & Thorne, R. M. (2003). Relativistic electron pitch-angle scattering by electromagnetic ion cyclotron waves during geomagnetic storms. *Journal of Geophysical Research*, *108*, 1143. https://doi.org/10.1029/2002JA009489

Summers, D., Ma, C., Meredith, N. P., Horne, R. B., Thorne, R. M., Heynderickx, D., & Anderson, R. R. (2002). Model of the energization of outer-zone electrons by whistler-mode chorus during the October 9, 1990 geomagnetic storm. *Geophysical Research Letters*, *29*(24), 2174. https://doi.org/10.1029/2002GL016039

Summers, D., Ni, B., & Meredith, N. P. (2007). Timescales for radiation belt electron acceleration and loss due to resonant wave-particle interactions: 2. Evaluation for VLF chorus, ELF hiss, and electromagnetic ion cyclotron waves. *Journal of Geophysical Research*, *112*, A04207. https://doi.org/10.1029/2006JA011993

Summers, D., Ni, B., Meredith, N. P., Horne, R. B., Thorne, R. M., Moldwin, M. B., & Anderson, R. R. (2008). Electron scattering by whistler-mode elf hiss in plasmaspheric plumes. *Journal of Geophysical Research*, *113*, A04219. https://doi.org/10.1029/2007JA012678

Summers, D., Thorne, R. M., & Xiao, F. (1998). Relativistic theory of wave-particle resonant diffusion with application to electron acceleration in the magnetosphere. *Journal of Geophysical Research*, *103*, 20487. https://doi.org/10.1029/98JA01740

Thorne, R. M., & Kennel, C. F. (1971). Relativistic electron precipitation during magnetic storm main phase. *Journal of Geophysical Research*, *76*, 4446–4453. https://doi.org/10.1029/JA076i019p04446

Thorne, R. M., Li, W., Ni, B., Ma, Q., Bortnik, J., Chen, L., … Kanekal, S. G. (2013). Rapid local acceleration of relativistic radiation-belt electrons by magnetospheric chorus. *Nature*, *504*, 411–414. https://doi.org/10.1038/nature12889

Tsurutani, B. T., Lakhina, G. S., & Verkhoglyadova, O. P. (2013). Energetic electron (>10 keV) microburst precipitation, ~5–15 s X-ray pulsations, chorus, and wave-particle interactions: A review. *Journal of Geophysical Research: Space Physics*, *118*, 2296–2312. https://doi.org/10.1002/jgra.50264

Tsyganenko, N. A., & Sitnov, M. I. (2005). Modeling the dynamics of the inner magnetosphere during strong geomagnetic storms. *Journal of Geophysical Research*, *110*, A03208. https://doi.org/10.1029/2004JA010798

Turner, D. L., Angelopoulos, V., Morley, S. K., Henderson, M. G., Reeves, G. D., Li, W., … Rodriguez, J. V. (2014). On the cause and extent of outer radiation belt losses during the 30 September 2012 dropout event. *Journal of Geophysical Research: Space Physics*, *119*, 1530–1540. https://doi.org/10.1002/2013JA019446

Turner, D. L., Shprits, Y., Hartinger, M., & Angelopoulos, V. (2012). Explaining sudden losses of outer radiation belt electrons during geomagnetic storms. *Nature Physics*, *8*, 208–212. https://doi.org/10.1038/nphys2185

Ukhorskiy, A. Y., Anderson, B. J., Takahashi, K., & Tsyganenko, N. A. (2006). Impact of ULF oscillations in solar wind dynamic pressure on the outer radiation belt electrons. *Geophysical Research Letters*, *33*, L06111. https://doi.org/10.1029/2005GL024380

Usanova, M. E., Drozdov, A., Orlova, K., Mann, I. R., Shprits, Y., Robertson, M. T., … Wygant, J. (2014). Effect of EMIC waves on relativistic and ultrarelativistic electron populations: Ground-based and Van Allen Probes observations. *Geophysical Research Letters*, *41*, 1375–1381. https://doi.org/10.1002/2013GL059024

Wang, B., Su, Z., Zhang, Y., Shi, S., & Wang, G. (2016). Nonlinear Landau resonant scattering of near-equatorially mirroring radiation belt electrons by oblique EMIC waves. *Geophysical Research Letters*, *43*, 3628–3636. https://doi.org/10.1002/2016GL068467

Wygant, J., Bonnell, J., Goetz, K., Ergun, R., Mozer, F., Bale, S., … Tao, J. (2013). The electric field and waves instruments on the radiation belt storm probes mission. *Space Sci. Rev.*, *179*(1–4), 183–220. https://doi.org/10.1007/s11214-013-0013-7

Yang, C., Su, Z., Xiao, F., Zheng, H., Wang, Y., Wang, S., … Funsten, H. (2016). Rapid flattening of butterfly pitch angle distributions of radiation belt electrons by whistler-mode chorus. *Geophysical Research Letters*, *43*, 8339–8347. https://doi.org/10.1002/2016GL070194

Zhang, J., Halford, A. J., Saikin, A. A., Huang, C.-L., Spence, H. E., Larsen, B. A., … Baker, D. N. (2016). EMIC waves and associated relativistic electron precipitation on 25–26 January 2013. *Journal of Geophysical Research: Space Physics*, *121*, 11,086–11,100. https://doi.org/10.1002/2016JA022918

Zhang, J.-C., Saikin, A. A., Kistler, L. M., Smith, C. W., Spence, H. E., Mouikis, C. G., … Jordanova, V. K. (2014). Excitation of EMIC waves detected by the Van Allen Probes on 28 April 2013. *Geophysical Research Letters*, *41*, 4101–4108. https://doi.org/10.1002/2014GL060621

Zhang, X.-J., Li, W., Thorne, R. M., Angelopoulos, V., Ma, Q., Li, J., … Fennell, J. F. (2016). Physical mechanism causing rapid changes in ultrarelativistic electron pitch angle distributions right after a shock arrival: Evaluation of an electron dropout event. *Journal of Geophysical Research: Space Physics*, *121*, 8300–8316. https://doi.org/10.1002/2016JA022517

Zhu, H., Su, Z., Xiao, F., Zheng, H., Wang, Y., Shen, C., … Baker, D. N. (2015). Plasmatrough exohiss waves observed by Van Allen Probes: Evidence for leakage from plasmasphere and resonant scattering of radiation belt electrons. *Geophysical Research Letters*, *42*, 1012–1019. https://doi.org/10.1002/2014GL062964